

PROJECTED SOBOLEV NATURAL GRADIENT DESCENT FOR NEURAL VARIATIONAL MONTE CARLO SOLUTION OF THE GROSS-PITAEVSKII EQUATION

CHENGLONG BAO*, CHEN CUI*, KAI JIANG†, AND SHI SHU†

Abstract. This paper proposes a neural variational Monte Carlo method based on deep neural networks to solve the Gross-Pitaevskii equation (GPE) via projected Sobolev natural gradient descent (NGD). Adopting an “optimize-then-discretize” strategy, we first apply a constraint-preserving continuous Riemannian gradient flow on an infinite-dimensional Riemannian manifold, which is subsequently mapped to the neural network parameter space via Galerkin projection. This process naturally induces a Sobolev energy metric that incorporates physical information, effectively mitigating stiffness during optimization. To address the explicit dependence on the normalization constant caused by the nonlinear interaction term in the GPE, we design a hybrid sampling strategy combining an integration stream and a MCMC stream to achieve precise estimation of the generalized Gram matrix and energy gradients. Numerical experiments on benchmark cases, including the harmonic oscillator potential in the strong interaction limit and multi-scale optical lattice potentials, demonstrate the high accuracy of the proposed method. Furthermore, it achieves an order-of-magnitude acceleration in convergence compared to standard optimizers like Adam, exhibiting superior robustness in handling strong nonlinearities and complex geometric constraints.

Key words. Gross-Pitaevskii Equation, Deep Neural Networks, Variational Monte Carlo, Riemannian Optimization, Natural Gradient Descent, Sobolev Gradient Flow

MSC codes. 65N30, 65K10, 81Q05, 68T07

1. Introduction. Bose-Einstein condensation (BEC) is a macroscopic quantum phenomenon emerging when a large number of identical bosons occupy a single quantum ground state at ultracold temperatures. Since its first experimental realization in 1995 [1], BEC has become a vital platform for exploring macroscopic quantum effects, superfluidity, and quantum simulation. Under the mean-field approximation, the macroscopic wave function (or order parameter) of a BEC is governed by the Gross-Pitaevskii equation (GPE) [29]. This nonlinear Schrödinger equation features a nonlinear term arising from effective contact interactions between atoms. Determining the ground state of the GPE is central to theoretical and numerical research. Mathematically, this corresponds to finding the global minimum of an energy functional on a Riemannian manifold, subject to a wave function normalization constraint (representing particle number conservation). However, due to the nonlinearity, the GPE energy functional is significantly non-convex, posing severe challenges for numerical computation.

Classical numerical methods for computing the GPE ground state generally fall into two categories. The first follows a “discretize-then-solve” approach, transforming the problem into a nonlinear eigenvalue problem solved via algebraic algorithms such as self-consistent field iteration [17, 8] or inverse iteration [26]. The second adopts a direct variational perspective, minimizing energy subject to manifold constraints. Representative methods include gradient flow with discrete normalization [5], projected Sobolev gradient methods [19, 13, 23, 11], Riemannian conjugate gradient optimization [2, 14, 35], momentum acceleration algorithms [10], and preconditioning

*Yau Mathematical Sciences Center, Tsinghua University, Beijing, China, 100084.(Corresponding author: chencui@mail.tsinghua.edu.cn)

†Hunan Key Laboratory for Computation and Simulation in Science and Engineering, Key Laboratory of Intelligent Computing and Information Processing of Ministry of Education, School of Mathematics and Computational Science, Xiangtan University, Xiangtan, Hunan, China, 411105.

techniques [2, 18]. A comprehensive review is provided in Ref. [22]. Despite their success, these classical solvers face significant bottlenecks. First, in regimes such as the strong interaction limit or highly inhomogeneous potentials, convergence rates deteriorate, and solvers are prone to entrapment in local minima [34]. Second, regarding the curse of dimensionality, while single-component BECs are typically three-dimensional, multi-component systems or those requiring high spatial resolution to resolve vortex cores demand excessive computational resources. Consequently, there is an urgent need for robust, computationally efficient algorithms.

Recently, deep neural networks (DNNs) have revitalized scientific computing through their powerful approximation capabilities and adaptability to high dimensions [37, 16, 42, 41]. Integrating neural networks into quantum wave function representations—termed “neural quantum states”—has emerged as a promising avenue to overcome traditional bottlenecks. In quantum many-body physics, neural variational Monte Carlo (neural VMC) methods [9] have successfully solved the Schrödinger equation for fermionic systems, exemplified by FermiNet [36] and PauliNet [25]. Concurrently, deep learning has advanced in addressing the specific topological structures of the GPE. Bao et al. [4] proposed the normalized deep neural network (Norm-DNN), which enforces the unit modulus constraint within the architecture, avoiding optimization difficulties associated with soft penalty terms commonly used in physics-informed neural networks (PINNs) [37]. Addressing the complex energy landscapes of rotating BECs, Kong et al. [28] developed a virtual rotation acceleration strategy within an operator learning framework, utilizing curriculum learning to guide the network across phase transitions and capture topological defects.

Despite these prospects, training DNNs to solve the GPE remains a high-dimensional non-convex optimization problem. Standard stochastic gradient descent and variants like Adam [27], while accessible, are often inefficient for quantum wave functions because the Euclidean geometry of parameter space fails to reflect the wave function’s curvature on the Riemannian manifold. In VMC, stochastic reconfiguration (SR) [39] has proven highly effective. SR is essentially equivalent to natural gradient descent (NGD) under the L^2 metric [3], employing the Fisher information matrix as the Riemannian metric to optimize step sizes on the manifold. Recently, Armegioiu et al. [3] established a unified geometric framework connecting parameter space algorithms with classical function space algorithms via Galerkin projection, though this was limited to linear problems. Substantial research [31, 43, 7, 33, 38, 6, 21, 15] has also focused on improving NGD efficiency and stability in PINNs and many-body systems. However, most existing NGD methods focus on simple PDEs; extending them to the GPE while maintaining normalization constraints via Riemannian gradient flows remains a frontier requiring in-depth exploration.

This paper aims to establish an efficient, accurate, and geometrically grounded deep learning algorithm for solving the GPE ground state. We propose a neural VMC method based on projected Sobolev NGD. Our main contributions are:

1. **Unified theoretical framework:** Adopting an “optimize-then-discretize” strategy, we first apply a continuous Sobolev gradient flow that preserves normalization on an infinite-dimensional Riemannian manifold. We then map this to the neural network parameter space via Galerkin projection, establishing an intrinsic link between continuous geometric flows and discrete natural gradient algorithms.
2. **Sobolev natural gradient:** To address the stiffness of the GPE energy functional, we introduce a parameter-space Sobolev metric related to the second-order variation of energy (specifically, a metric based on the energy

inner product).

3. **Nonlinearity-adapted VMC algorithm:** To manage the explicit dependence on the normalization constant caused by the nonlinear interaction term, we design a hybrid sampling strategy. This combines deterministic integration with Markov chain Monte Carlo (MCMC) sampling to accurately estimate energy gradients containing normalization factors, deriving a generalized Gram matrix that includes “drift-gradient coupling” terms.
4. **Numerical verification:** We validate the algorithm on challenging benchmarks, such as the strong interaction limit and multi-scale optical lattice potentials. Experimental results demonstrate that our method achieves an order-of-magnitude acceleration in convergence compared to first-order optimizers like Adam.

The remainder of this paper is organized as follows: Section 2 reviews the GPE model, variational properties, and neural network parameterization. Section 3 details the “optimize-then-discretize” strategy, introducing Sobolev gradient flow theory on infinite-dimensional Riemannian manifolds and deriving the natural gradient dynamics in parameter space. Section 4 covers numerical implementation via VMC, focusing on statistical gradient estimation, the hybrid sampling strategy, and efficient Sobolev Gram matrix computation. Section 5 presents numerical results and performance comparisons. Finally, Section 6 summarizes the work and outlines future research directions.

2. Preliminaries and Problem Definition. This section first introduces the GPE describing the macroscopic dynamics of BEC and its variational structure, followed by defining the deep neural network model used for wave function parameterization.

2.1. Gross-Pitaevskii Equation. The GPE is the cornerstone of mean-field theory for describing the macroscopic dynamics of BECs. Under extremely low temperature conditions ($T \rightarrow 0$), a large number of identical bosons in a dilute Bose gas condense into the same single-particle quantum ground state, and their microscopic many-body interactions can be renormalized into an effective nonlinear mean-field contact potential.

For an interacting Bose gas with mass m confined by an external potential $V_{\text{ext}}(\mathbf{r})$, its order parameter (i.e., macroscopic wave function) $\Psi(\mathbf{r}, t)$ follows the time-dependent nonlinear Schrödinger equation

$$i\hbar \frac{\partial \Psi}{\partial t} = \left(-\frac{\hbar^2}{2m} \nabla^2 + V_{\text{ext}}(\mathbf{r}) + g|\Psi|^2 \right) \Psi(\mathbf{r}, t),$$

where $g = \frac{4\pi\hbar^2 a_s}{m}$ describes the effective interaction strength between particles (a_s is the s-wave scattering length). To find the steady-state solution, letting $\Psi(\mathbf{r}, t) = \Psi(\mathbf{r})e^{-i\mu t/\hbar}$ (where μ is the chemical potential), we obtain the following nonlinear eigenvalue problem

$$\mu \Psi(\mathbf{r}) = -\frac{\hbar^2}{2m} \nabla^2 \Psi(\mathbf{r}) + V_{\text{ext}}(\mathbf{r}) \Psi(\mathbf{r}) + g|\Psi(\mathbf{r})|^2 \Psi(\mathbf{r}).$$

To facilitate numerical computation and unify mathematical notation, a characteristic length x_s (e.g., harmonic oscillator length) and characteristic energy $\hbar\omega$ are usually introduced to dimensionless the equation. Defining dimensionless variables $\mathbf{r}' = \mathbf{r}/x_s$ and the renormalized wave function $\psi = \Psi \sqrt{x_s^3/N}$ such that the dimen-

sionless wave function satisfies the normalization condition $\|\psi\|^2 = 1$. Substituting and rearranging (and omitting primes), we obtain the following dimensionless Gross-Pitaevskii energy functional

$$(2.1) \quad E(\psi) = \int_{\mathcal{D}} \left(\frac{1}{2} |\nabla \psi(\mathbf{r})|^2 + V(\mathbf{r}) |\psi(\mathbf{r})|^2 + \frac{\beta}{2} |\psi(\mathbf{r})|^4 \right) d\mathbf{r},$$

where $\beta = \frac{4\pi N a_s}{x_s}$ is the dimensionless interaction parameter ($\beta > 0$ corresponds to repulsive interaction, $\beta < 0$ corresponds to attractive interaction); this paper mainly considers the case $\beta > 0$. $V(\mathbf{r})$ is the given real-valued potential function, typically satisfying the confinement condition $\lim_{|\mathbf{r}| \rightarrow \infty} V(\mathbf{r}) = +\infty$. The computational domain is usually taken as $\mathcal{D} = [-a, a]^d$. When a is sufficiently large, due to the exponential decay of the wave function at the boundaries under strong confinement, assuming zero boundary conditions $\psi|_{\partial\mathcal{D}} = 0$ is a reasonable approximation.

The ground state ψ_{GS} can be obtained by solving the following constrained minimization problem

$$(2.2) \quad \psi_{\text{GS}} = \arg \min_{\psi \in \mathbb{S}} E(\psi), \quad \mathbb{S} := \left\{ \psi \in H_0^1(\mathcal{D}) : \|\psi\|_{L^2(\mathcal{D})}^2 = \int_{\mathcal{D}} |\psi|^2 d\mathbf{r} = 1 \right\}.$$

Since the constraint set \mathbb{S} constitutes a Riemannian manifold in Hilbert space, solving for the ground state can also be viewed as an optimization problem on a nonlinear Riemannian manifold. The existence of the ground state is guaranteed by the property that the energy functional $E(\psi)$ is bounded below on the manifold \mathbb{S} and is weakly lower semicontinuous in $H_0^1(\mathcal{D})$. Specifically, since the potential function V is bounded below (i.e., $V(\mathbf{r}) \geq V_{\min}$), the energy functional satisfies the coercivity condition

$$E(\psi) \geq \frac{1}{2} \int_{\mathcal{D}} V |\psi|^2 d\mathbf{r} \geq \frac{1}{2} V_{\min}.$$

Introducing the Lagrange multiplier μ (physically corresponding to the chemical potential), we define the Lagrangian

$$\mathcal{L}(\psi, \mu) = E(\psi) - \mu \left(\int_{\mathcal{D}} |\psi|^2 d\mathbf{r} - 1 \right).$$

The Fréchet derivative $\langle E'(\psi), v \rangle$ of the energy functional E is calculated as

$$(2.3) \quad \langle E'(\psi), v \rangle = \frac{d}{d\varepsilon} E(\psi + \varepsilon v) \Big|_{\varepsilon=0} = \int_{\mathcal{D}} (\nabla \psi \cdot \nabla v + 2V\psi v + 2\beta\psi^3 v) d\mathbf{r}.$$

From the Euler-Lagrange equation condition $\delta \mathcal{L} = \langle E'(\psi), v \rangle - \mu \cdot 2(\psi, v)_{L^2} = 0$, and adjusting coefficients, we obtain the weak form of the GPE eigenvalue problem

$$\int_{\mathcal{D}} \left(\frac{1}{2} \nabla \psi \cdot \nabla v + V\psi v + \beta\psi^3 v \right) d\mathbf{r} = \mu \int_{\mathcal{D}} \psi v d\mathbf{r}, \quad \forall v \in H_0^1(\mathcal{D}).$$

The corresponding nonlinear Schrödinger eigenvalue problem (strong form) is

$$(2.4) \quad H[\psi]\psi := \left(-\frac{1}{2} \nabla^2 + V(\mathbf{r}) + \beta|\psi|^2 \right) \psi = \mu\psi.$$

The ground state possesses the following properties:

- The minimum eigenvalue μ_1 and the ground state energy E satisfy the relation $\mu_1 = E(\psi_{\text{GS}}) + \frac{\beta}{2} \|\psi_{\text{GS}}\|_{L^4}^4$, reflecting the contribution of the nonlinear interaction energy.
- The corresponding eigenfunction $\psi_{\text{GS}} \in \mathbb{S}$ is unique up to a phase factor.
- ψ_{GS} is continuous and non-zero within the domain \mathcal{D} ; therefore, $\psi_{\text{GS}}(\mathbf{r}) > 0$ is usually selected as the physical ground state solution.

2.2. Deep Neural Networks. Traditional discretization methods (such as finite element methods, spectral methods [45]) face exponential growth in computational complexity with dimensionality when solving high-dimensional problems, known as the “curse of dimensionality”. To overcome this bottleneck, we employ DNNs as the parameterization ansatz for the wave function. According to the Universal Approximation Theorem [12], as long as the network has sufficient width or depth, a DNN with non-polynomial activation functions can approximate continuous functions on a compact set with arbitrary precision. This makes DNNs a highly promising mesh-free high-dimensional function approximator.

2.2.1. Fully Connected Network Architecture. Given that the ground state wave function is a real-valued function, this paper primarily uses fully connected neural networks, also known as multi-layer perceptrons (MLP), to construct the parameterized mapping of the wave function $f_\theta : \mathbb{R}^d \rightarrow \mathbb{R}$. For input spatial coordinates $\mathbf{r} \in \mathbb{R}^d$, the forward propagation process of an FNN containing L layers is recursively defined as

$$(2.5) \quad \begin{aligned} \mathbf{h}^{(0)} &= \mathbf{r}, \\ \mathbf{h}^{(l)} &= \sigma \left(\mathbf{W}^{(l)} \mathbf{h}^{(l-1)} + \mathbf{b}^{(l)} \right), \quad l = 1, \dots, L-1, \\ \psi_\theta(\mathbf{r}) &= \mathbf{W}^{(L)} \mathbf{h}^{(L-1)} + \mathbf{b}^{(L)}. \end{aligned}$$

Here, $\theta = \{\mathbf{W}^{(l)}, \mathbf{b}^{(l)}\}_{l=1}^L \in \mathbb{R}^P$ constitutes the set of trainable parameters of the network. $\mathbf{W}^{(l)}$ and $\mathbf{b}^{(l)}$ represent the weight matrix and bias vector of the l -th layer, respectively.

2.2.2. Normalization Strategy for Neural Network Wave Functions. When solving the GPE using neural networks, the parameter optimization process is carried out in the Euclidean space \mathbb{R}^P , while the physical wave function normalization constraint requires the solution to strictly lie on the unit sphere \mathbb{S} . Effectively bridging the gap between unconstrained optimization in parameter space and geometric constraints in function space to achieve efficient and stable normalization is a core difficulty in algorithm design. Currently, mainstream strategies fall into three main categories:

1. **Soft Constraints:**

- **Method:** Based on the Lagrange multiplier idea, a penalty term is introduced into the loss function $\mathcal{L}_{\text{total}} = E(\psi_\theta) + \lambda (\|\psi_\theta\|_{L^2}^2 - 1)^2$.
- **Limitations:** This method introduces an additional hyperparameter λ and is extremely sensitive to its selection. If λ is too small, normalization error cannot be eliminated, violating physical conservation laws; if λ is too large, it causes the loss function landscape to become extremely steep and rugged, making the optimization process numerically unstable and prone to particle number drift during training.

2. **Scale-Invariant Approach (Based on Rayleigh Quotient VMC):**

- **Principle:** Widely used in solving **linear** many-body Schrödinger equations (e.g., FermiNet [36]). This method utilizes the scale invariance of the linear operator Rayleigh quotient $R(\psi) = \langle \psi | \hat{H} | \psi \rangle / \langle \psi | \psi \rangle$ to directly optimize the unnormalized network output.
- **Limitations:** This method cannot be directly applied to the GPE. Since the GPE energy functional contains high-order nonlinear interaction terms (e.g., $\frac{\beta}{2} |\psi|^4$), its energy no longer possesses scale invariance, so the normalization constant must be explicitly handled.

3. Hard Constraints:

- **Method:** Construct a forcibly normalized ansatz $\hat{\psi}_\theta(\mathbf{r}) = \frac{\psi_\theta(\mathbf{r})}{\|\psi_\theta\|_{L^2}}$. During computation, the norm $\|\psi_\theta\|_{L^2}$ is calculated in real-time via numerical integration or statistical estimation, and division is performed [4, 28].
- **Pros/Cons:** The advantage is that it strictly guarantees the wave function satisfies physical constraints throughout the optimization, avoiding interaction energy calculation errors caused by modulus estimation bias. However, directly applying automatic differentiation to a normalization factor containing an integral significantly increases the complexity of the computational graph and can easily trigger gradient explosion or vanishing, leading to training instability.

In summary, given the nonlinear nature of the GPE, this paper adopts a strategy combining **explicit normalization with VMC sampling**. This hybrid strategy utilizes the efficiency of VMC in adaptively handling high-dimensional integrals while strictly satisfying the normalization constraint through an explicit structure. Crucially, through the statistical estimation form of gradients (using the log-derivative trick), we avoid the normalization constant directly participating in the construction of the backpropagation computational graph, thereby eliminating gradient instability and significantly improving the algorithm’s numerical stability and computational efficiency.

3. Riemannian Optimization and Neural Discretization. This section employs an “optimize-then-discretize” strategy to construct the solution algorithm. We first construct a continuous-time Sobolev gradient flow on an infinite-dimensional Hilbert space based on Riemannian manifold geometry; then, using the Galerkin projection principle, we discretize it into a NGD method in the neural network parameter space.

3.1. Continuous Sobolev Gradient Flow. We briefly review the Riemannian Sobolev gradient flow method (see [22] for details). The goal is to construct a dynamical system that monotonically decreases the energy $E(\psi)$ while strictly preserving the mass constraint $\|\psi\|_{L^2} = 1$. This is essentially a constrained optimization problem defined on the Riemannian manifold \mathbb{S} . In the unconstrained case, the variation of the energy functional is given by the Fréchet derivative $E'(\psi)$ (2.3). To handle the spherical geometric constraint, $E'(\psi)$ needs to be projected onto the tangent space at ψ

$$T_\psi \mathbb{S} = \{v \in H_0^1(\mathcal{D}) : (\psi, v)_{L^2} = \int_{\mathcal{D}} \psi v \, d\mathbf{r} = 0\}.$$

This projected gradient is referred to as the **Riemannian Gradient**.

However, the Fréchet derivative $E'(\psi)$ is an element of the dual space $H^{-1}(\mathcal{D})$, while the tangent space is a subset of the primal space $H_0^1(\mathcal{D})$. To perform projection,

one must first use the Riesz representation theorem to represent $E'(\psi)$ in a subspace X of L^2 , and this “dual avatar” is the Sobolev gradient.

Definition of Sobolev Gradient. Let X be a Hilbert space equipped with inner product $(\cdot, \cdot)_X$, and let X be compactly embedded in $L^2(\mathcal{D})$. The X -Sobolev gradient of the functional E at ψ , denoted $\nabla_X E(\psi) \in X$, is defined as the unique function satisfying the following Riesz representation relation

$$(3.1) \quad (\nabla_X E(\psi), \phi)_X = \langle E'(\psi), \phi \rangle, \quad \forall \phi \in X.$$

Here $\langle \cdot, \cdot \rangle$ denotes the dual pairing. $\nabla_X E(\psi)$ represents the direction of steepest energy ascent under the metric geometry of space X .

Four Typical Sobolev Gradients. Different choices of metric space X and its inner product correspond to different gradient flows, leading to algorithms with varying numerical stability and convergence rates

1. **L^2 -Sobolev Gradient:** Choose $X = L^2(\mathcal{D})$ with standard L^2 inner product.

$$(3.2) \quad \nabla_{L^2} E(\psi) = H[\psi]\psi = \left(-\frac{1}{2}\nabla^2 + V + \beta|\psi|^2 \right) \psi.$$

The corresponding gradient flow is the classic imaginary time evolution method [5].

2. **H^1 -Sobolev Gradient:** Choose $X = H_0^1(\mathcal{D})$ with standard H^1 inner product $(u, v)_{H^1} = (\nabla u, \nabla v)_{L^2} + (u, v)_{L^2}$. The gradient $\nabla_{H^1} E(\psi)$ is obtained by solving the Poisson equation

$$(3.3) \quad (-\nabla^2 + I)\nabla_{H^1} E(\psi) = \nabla_{L^2} E(\psi).$$

The H^1 gradient acts as a low-pass filter (smoothing) on the L^2 gradient, significantly improving the condition number of the algorithm under mesh discretization.

To further accelerate convergence, one can utilize second-order information of the problem to construct an inner product approximating the Hessian matrix of the energy functional. Define the parameterized bilinear form $a_\psi(\cdot, \cdot)$

$$(3.4) \quad a_\psi(v, w) := \int_{\mathcal{D}} \left(\frac{1}{2}\nabla v \cdot \nabla w + Vvw + \beta|\psi|^2vw \right) \mathrm{d}\mathbf{r}.$$

3. **a_0 -Sobolev Gradient** (Linear Preconditioning): $X = H_0^1(\mathcal{D})$, equipped with the inner product defined by $a_0(\cdot, \cdot)$ (taking the non-interacting Hamiltonian with $\psi = 0$).

$$(3.5) \quad a_0(\nabla_{a_0} E(\psi), \phi) = \langle E'(\psi), \phi \rangle.$$

This is equivalent to preconditioning with the inverse of the linear operator at each step.

4. **a_ψ -Sobolev Gradient** (Nonlinear Preconditioning): $X = H_0^1(\mathcal{D})$, equipped with the inner product $a_\psi(\cdot, \cdot)$ dependent on the current state ψ .

$$(3.6) \quad a_\psi(\nabla_{a_\psi} E(\psi), \phi) = \langle E'(\psi), \phi \rangle.$$

This gradient flow approximates Newton’s method and converges fastest when nonlinearity is strong.

Riemannian Projection and Metric Compatibility. To satisfy the spherical constraint $\|\psi\|_{L^2} = 1$, we must project the unconstrained Sobolev gradient $\nabla_X E(\psi)$ back onto the tangent space $T_\psi \mathbb{S}$. A key issue of metric compatibility arises here: the constraint is defined under the L^2 norm, while the gradient is calculated under the metric of a general space X . If simple L^2 orthogonal projection $v - (v, \psi)_{L^2} \psi$ is used, direction bias will occur for non- L^2 gradients (such as H^1 or a_ψ), destroying the energy-decreasing property.

The correct Riemannian gradient $\text{grad}_X E(\psi)$ must use the generalized orthogonal projection operator $P_{\psi, X}$ with respect to the inner product $(\cdot, \cdot)_X$

$$(3.7) \quad \text{grad}_X E(\psi) = P_{\psi, X}(\nabla_X E) = \nabla_X E - \frac{(\nabla_X E, n_\psi)_X}{\|n_\psi\|_X^2} n_\psi.$$

Here, $n_\psi \in X$ is the Riesz representation of the differential of the constraint functional in space X (i.e., the normal vector to the constraint surface), satisfying

$$(n_\psi, \phi)_X = (\psi, \phi)_{L^2}, \quad \forall \phi \in X.$$

Only when $X = L^2$ does $n_\psi = \psi$; in other spaces, n_ψ must be obtained by solving the corresponding linear equation.

In summary, the continuous-time projected Sobolev gradient flow is

$$(3.8) \quad \frac{\partial \psi}{\partial t} = -\text{grad}_X E(\psi(t)).$$

This dynamical system strictly satisfies mass conservation $\|\psi(t)\|_{L^2} \equiv 1$ and monotonically decreases energy. Physically, the coefficient introduced by the projection term $\mu(t) = (\nabla_X E, n_\psi)_X / \|n_\psi\|_X^2$ corresponds exactly to the time-evolving chemical potential.

Remark 3.1. Besides the aforementioned first-order ODE-based Sobolev gradient flows, there are many other efficient computational techniques in the field of BEC ground state calculation:

1. 2nd-Order ODE based Methods [10]

- Introducing virtual mass or inertia terms to construct a second-order dynamical system

$$\beta \frac{d^2 \psi}{dt^2} + \frac{d \psi}{dt} = -\text{grad} E(\psi)$$

- **Advantage:** Similar to Nesterov momentum acceleration, it can utilize inertia to overcome slow convergence of first-order gradient flows in flat energy landscape regions and helps escape shallow local minima.

2. Riemannian Conjugate Gradient (RCG) [14]

- Extends the classical conjugate gradient method to the Riemannian manifold \mathbb{S} .
- **Key Technique:** Utilizes vector transport to parallel transport the search direction from the previous step $T_{\psi_n} \mathbb{S}$ to the current tangent space $T_{\psi_{n+1}} \mathbb{S}$ to maintain conjugacy.
- **Advantage:** Generally possesses superlinear convergence, superior to the linear convergence of steepest descent.

3. Preconditioned Normalized L^2 -Gradient Flow [2]

- Explicitly discretizes the L^2 -gradient flow and applies a preconditioner M directly before projection/normalization

$$\tilde{\psi}^{(n+1)} = \psi^{(n)} - \tau M \nabla_{L^2} E(\psi^{(n)}), \quad \psi^{(n+1)} = \frac{\tilde{\psi}^{(n+1)}}{\|\tilde{\psi}^{(n+1)}\|}$$

- **Advantage:** No complex Riemannian geometry derivation required, simple implementation. When M is chosen appropriately (e.g., $M \approx (-\nabla^2 + V)^{-1}$), the effect approaches that of H^1 -gradient flow.

3.2. Neural Network Parameterization and Natural Gradient Optimization. To numerically solve the infinite-dimensional geometric gradient flow derived in the previous section, we restrict the wave function to a finite-dimensional submanifold parameterized by a normalized deep neural network. Using the Galerkin projection method, the continuous dynamics in function space are mapped to ODEs in parameter space θ , leading to the NGD method.

3.2.1. Galerkin Projection. First, we define the normalized neural network wave function manifold parameterized by θ as $\mathcal{M}_\theta = \{\hat{\psi}_\theta \in \mathbb{S} : \theta \in \mathbb{R}^P\}$, with the normalization ansatz

$$\hat{\psi}_\theta(\mathbf{r}) = \frac{\psi_\theta(\mathbf{r})}{\|\psi_\theta\|_{L^2}}, \quad \theta \in \mathbb{R}^P.$$

Our goal is to project the continuous gradient flow equation (3.8) from the infinite-dimensional Hilbert space onto this finite-dimensional manifold \mathcal{M}_θ .

According to the chain rule, the time evolution rate of the wave function can be expanded as a linear combination of the parameter change rate $\dot{\theta}$

$$\partial_t \hat{\psi}_\theta = \sum_{j=1}^P \frac{\partial \hat{\psi}_\theta}{\partial \theta_j} \dot{\theta}_j = J(\theta) \dot{\theta},$$

where $J(\theta) = [\partial_{\theta_1} \hat{\psi}, \dots, \partial_{\theta_P} \hat{\psi}]$ represents the Jacobian operator. Since $\hat{\psi}_\theta$ satisfies the normalization constraint, its partial derivatives with respect to parameters satisfy the orthogonality condition $\langle \hat{\psi}_\theta, \partial_{\theta_j} \hat{\psi}_\theta \rangle_{L^2} = 0$, which implies $\partial_{\theta_j} \hat{\psi}_\theta$ lies in the tangent space $T_{\hat{\psi}_\theta} \mathbb{S}$. Accordingly, we define the tangent space of the neural network manifold at the current parameters as

$$\mathcal{V}_\theta = \text{span} \left\{ \frac{\partial \hat{\psi}_\theta}{\partial \theta_j}, j = 1, \dots, P \right\} \subset T_{\hat{\psi}_\theta} \mathbb{S}.$$

Limited by the expressivity of the neural network, the true gradient flow direction $-\text{grad}_X E(\hat{\psi}_\theta)$ usually does not lie entirely within the finite-dimensional tangent space \mathcal{V}_θ . Based on the Galerkin projection principle, we need to find an optimal tangent vector $J(\theta) \dot{\theta}$ to best approximate the target evolution direction. This is equivalent to requiring the dynamics residual to be orthogonal to the tangent space \mathcal{V}_θ under the metric X

$$(3.9) \quad \left\langle J(\theta) \dot{\theta} + \text{grad}_X E(\hat{\psi}_\theta), \frac{\partial \hat{\psi}_\theta}{\partial \theta_j} \right\rangle_X = 0, \quad \forall j = 1, \dots, P.$$

3.2.2. Natural Gradient Flow Equation. Expanding (3.9), we obtain a linear system in parameter space

$$\sum_{i=1}^P \dot{\theta}_i \left\langle \frac{\partial \hat{\psi}_\theta}{\partial \theta_i}, \frac{\partial \hat{\psi}_\theta}{\partial \theta_j} \right\rangle_X = - \left\langle \text{grad}_X E(\hat{\psi}_\theta), \frac{\partial \hat{\psi}_\theta}{\partial \theta_j} \right\rangle_X, \quad j = 1, \dots, P.$$

Left-hand side (Metric Matrix): Define $G(\theta)$ as the **Gram matrix** induced by the X -inner product

$$(3.10) \quad G_{ij}(\theta) = \left\langle \frac{\partial \hat{\psi}_\theta}{\partial \theta_i}, \frac{\partial \hat{\psi}_\theta}{\partial \theta_j} \right\rangle_X.$$

This matrix acts as the Riemannian metric tensor on the parameter manifold, characterizing the distance change of the wave function in space X caused by parameter perturbations.

Right-hand side (Gradient Map): Using the properties of the Riemannian gradient projection operator and the definition of the Sobolev gradient (3.1), the right-hand side can be simplified to the form of the Euclidean gradient. Since $\partial_{\theta_j} \hat{\psi}_\theta$ belongs to the tangent space, the projection operator $P_{\psi, X}$ acts on it as identity, thus

$$\begin{aligned} \left\langle \text{grad}_X E, \partial_{\theta_j} \hat{\psi}_\theta \right\rangle_X &= \left\langle \nabla_X E, \partial_{\theta_j} \hat{\psi}_\theta \right\rangle_X \quad (\text{Self-adjointness of projection}) \\ &= \langle E'(\hat{\psi}_\theta), \partial_{\theta_j} \hat{\psi}_\theta \rangle \quad (\text{Riesz representation theorem}) \\ &= \frac{\partial}{\partial \theta_j} E(\hat{\psi}_\theta) = \nabla_\theta L(\theta)_j. \quad (\text{Chain rule}) \end{aligned}$$

Combining the above derivations, we obtain the natural gradient flow equation in parameter space

$$(3.11) \quad G(\theta) \dot{\theta} = -\nabla_\theta L(\theta).$$

3.2.3. Discretization and Physical Metric Selection. Applying the forward Euler method to discretize (3.11) in time, we obtain the NGD iteration scheme

$$(3.12) \quad \theta^{k+1} = \theta^k - \tau_k G(\theta^k)^{-1} \nabla_\theta L(\theta^k).$$

where τ_k is the learning rate. NGD uses $G(\theta)^{-1}$ to precondition the Euclidean gradient, eliminating the curvature effects of the parameterization and achieving steepest descent in the function space sense.

The choice of space X and its inner product determines the properties of the Gram matrix $G(\theta)$, thereby affecting the convergence behavior of the algorithm

- **L^2 Metric:** If $X = L^2$ is chosen, $G(\theta)$ degenerates to the standard Fisher information matrix. This corresponds to the traditional SR method [39].
- **Energy Metric:** In this paper, we employ an inner product related to the second-order properties of the energy functional (such as the a_ψ -inner product defined in (3.4)) to construct $G(\theta)$. This choice effectively introduces the Hessian information of the physical system into the optimization process, significantly mitigating stiffness in solving the GPE and accelerating convergence.

4. Numerical Implementation Based on VMC. This section details how to translate the aforementioned geometric gradient flow theory into a concrete numerical algorithm based on the VMC method. The core difficulty lies in handling the normalization constant dependency caused by nonlinear interactions and efficiently computing the Gram matrix.

4.1. Statistical Estimation of the Energy Functional. The theoretical basis for the variational solution is the Ritz variational principle [20]. For a normalized trial wave function, its energy expectation is always an upper bound to the ground state energy E_g

$$(4.1) \quad E(\hat{\psi}) = \int_{\mathcal{D}} \left(\frac{1}{2} |\nabla \hat{\psi}|^2 + V(\mathbf{r}) |\hat{\psi}|^2 + \frac{\beta}{2} |\hat{\psi}|^4 \right) d\mathbf{r} \geq E_g.$$

This principle transforms the eigenvalue problem into an optimization problem of finding the optimal normalized function ψ in function space.

Define the normalization constant (partition function)

$$(4.2) \quad Z(\theta) = \|\psi_{\theta}\|_{L^2}^2 = \int_{\mathcal{D}} |\psi_{\theta}(\mathbf{r})|^2 d\mathbf{r}.$$

In the VMC framework, we transform the integral into an expectation with respect to the probability distribution $p_{\theta}(\mathbf{r})$

$$(4.3) \quad p_{\theta}(\mathbf{r}) = \frac{|\psi_{\theta}(\mathbf{r})|^2}{Z(\theta)} = |\hat{\psi}_{\theta}(\mathbf{r})|^2.$$

Although the Metropolis-Hastings (M-H) algorithm [32] allows generating samples $\mathbf{r} \sim p_{\theta}$ knowing only the unnormalized probability $|\psi_{\theta}|^2$, the nonlinear nature of GPE makes it impossible to completely avoid the calculation of $Z(\theta)$. Below we derive the expectation form of the energy functional (loss function), splitting it into linear and nonlinear interaction parts

• **Linear Part (Kinetic and Potential Energy):** Define the local energy as

$$E_L(\mathbf{r}; \theta) = \frac{-\frac{1}{2} \nabla^2 \psi_{\theta}(\mathbf{r}) + V(\mathbf{r}) \psi_{\theta}(\mathbf{r})}{\psi_{\theta}(\mathbf{r})}.$$

In its expectation $\mathbb{E}_{\mathbf{r} \sim p_{\theta}}[E_L(\mathbf{r})]$, the Z in the numerator and denominator cancels out automatically, requiring no explicit calculation.

• **Nonlinear Interaction Part:** This term is $E_{\text{int}} = \frac{\beta}{2} \int |\hat{\psi}_{\theta}|^4 d\mathbf{r} = \frac{\beta}{2Z(\theta)^2} \int |\psi_{\theta}|^4 d\mathbf{r}$.

Using the importance sampling identity $\int f = \int \frac{f}{p} p = \mathbb{E}_p[f/p]$, we have

$$\int_{\mathcal{D}} |\psi_{\theta}|^4 d\mathbf{r} = Z(\theta) \cdot \mathbb{E}_{\mathbf{r} \sim p_{\theta}} [|\psi_{\theta}(\mathbf{r})|^2].$$

Substituting back, we obtain the form explicitly dependent on $Z(\theta)$

$$E_{\text{int}} = \mathbb{E}_{\mathbf{r} \sim p_{\theta}} \left[\frac{\beta}{2Z(\theta)} |\psi_{\theta}(\mathbf{r})|^2 \right].$$

In summary, the total energy expectation of GPE is

$$(4.4) \quad E(\theta) = \mathbb{E}_{\mathbf{r} \sim p_{\theta}} \left[E_L(\mathbf{r}; \theta) + \frac{\beta}{2Z(\theta)} |\psi_{\theta}(\mathbf{r})|^2 \right].$$

This implies that besides estimating the expectation via MCMC sampling, the scalar $Z(\theta)$ must also be accurately calculated through deterministic integration.

4.2. Estimation of Energy Functional Gradient. To utilize gradient-based optimization algorithms (such as Adam or NGD), the gradient of the total energy with respect to parameters θ , $\nabla_\theta E(\theta)$, needs to be calculated. Due to the explicit dependence on the normalization constant $Z(\theta)$, this derivation is more complex than standard VMC.

We employ the log-derivative trick. Define the score function $O_\theta(\mathbf{r})$ as the gradient of the logarithm of the wave function modulus

$$(4.5) \quad O_\theta(\mathbf{r}) = \nabla_\theta \ln |\psi_\theta(\mathbf{r})| = \frac{\nabla_\theta |\psi_\theta(\mathbf{r})|}{|\psi_\theta(\mathbf{r})|}.$$

This yields the basic identity: $\nabla_\theta |\psi_\theta|^2 = 2|\psi_\theta|^2 O_\theta$.

We decompose the total energy $E(\theta)$ into the linear part E_{lin} (kinetic and external potential energy) and the nonlinear interaction part E_{int} for separate differentiation.

4.2.1. Gradient of the Linear Part. The linear energy term E_{lin} is essentially the quantum expectation (i.e., Rayleigh quotient) of the linear part of the Hamiltonian $\hat{H}_{\text{lin}} = -\frac{1}{2}\nabla^2 + V$ under the trial wave function

$$(4.6) \quad E_{\text{lin}}(\theta) = \frac{\langle \psi_\theta | \hat{H}_{\text{lin}} | \psi_\theta \rangle}{\langle \psi_\theta | \psi_\theta \rangle} = \frac{\mathcal{N}(\theta)}{Z(\theta)}.$$

To calculate its gradient $\nabla_\theta E_{\text{lin}}$, using the quotient rule for scalar functions $\nabla(u/v) = (v\nabla u - u\nabla v)/v^2$

$$(4.7) \quad \nabla_\theta E_{\text{lin}} = \frac{\nabla_\theta \mathcal{N}}{Z} - \frac{\mathcal{N}}{Z} \frac{\nabla_\theta Z}{Z} = \frac{\nabla_\theta \mathcal{N}}{Z} - E_{\text{lin}} \frac{\nabla_\theta Z}{Z}.$$

Calculating the gradients of the numerator \mathcal{N} and denominator Z respectively

1. **Denominator Gradient (Normalization Constant):** Using the identity $\nabla_\theta |\psi|^2 = 2|\psi|^2 O_\theta$

$$(4.8) \quad \nabla_\theta Z = \int \nabla_\theta |\psi|^2 \, d\mathbf{r} = \int 2|\psi|^2 O_\theta \, d\mathbf{r} = 2Z \mathbb{E}_{\mathbf{r} \sim p_\theta}[O_\theta].$$

2. **Numerator Gradient (Unnormalized Energy Expectation):** Since parameters θ are real and \hat{H}_{lin} is Hermitian, using the product rule for derivative operators

$$(4.9) \quad \begin{aligned} \nabla_\theta \mathcal{N} &= \nabla_\theta \langle \psi | \hat{H}_{\text{lin}} | \psi \rangle = 2 \operatorname{Re} \langle \nabla_\theta \psi | \hat{H}_{\text{lin}} | \psi \rangle \\ &= 2 \int |\psi(\mathbf{r})|^2 O_\theta(\mathbf{r}) \frac{\hat{H}_{\text{lin}} \psi(\mathbf{r})}{\psi(\mathbf{r})} \, d\mathbf{r} \\ &= 2Z \mathbb{E}_{\mathbf{r} \sim p_\theta}[O_\theta(\mathbf{r}) E_L(\mathbf{r})]. \end{aligned}$$

Substituting these two terms back into (4.7) and canceling the common factor Z

$$(4.10) \quad \begin{aligned} \nabla_\theta E_{\text{lin}} &= \frac{2Z \mathbb{E}[O_\theta E_L]}{Z} - E_{\text{lin}} \frac{2Z \mathbb{E}[O_\theta]}{Z} \\ &= 2(\mathbb{E}[E_L O_\theta] - \mathbb{E}[E_L] \mathbb{E}[O_\theta]). \end{aligned}$$

This is exactly the covariance form found in statistics

$$(4.11) \quad \nabla_\theta E_{\text{lin}} = 2 \operatorname{Cov}_{p_\theta}(E_L, O_\theta).$$

Note: The above derivation also explains the physical origin of the aforementioned identity $\nabla_\theta p_\theta = p_\theta \nabla_\theta \ln p_\theta$. Since $\ln p_\theta = \ln |\psi|^2 - \ln Z$, its gradient is $\nabla \ln p_\theta = 2(O_\theta - \mathbb{E}[O_\theta])$, which corresponds exactly to the centering term in the covariance.

4.2.2. Gradient of the Nonlinear Interaction Part. The interaction energy E_{int} is defined as

$$(4.12) \quad E_{\text{int}}(\theta) = \frac{\beta}{2} \int_{\mathcal{D}} |\hat{\psi}_\theta|^4 \, d\mathbf{r} = \frac{\beta}{2} \frac{N_4(\theta)}{Z(\theta)^2},$$

which contains two integral terms: the fourth-order moment integral $N_4(\theta) = \int |\psi_\theta|^4 \, d\mathbf{r}$ and the normalization constant $Z(\theta)$.

Step 1: Expansion using Quotient Rule. Apply the quotient rule to E_{int}

$$(4.13) \quad \nabla_\theta E_{\text{int}} = \frac{\beta}{2} \frac{Z^2(\nabla_\theta N_4) - N_4(\nabla_\theta Z^2)}{Z^4} = \frac{\beta}{2Z^2} \left[\nabla_\theta N_4 - 2 \frac{N_4}{Z} \nabla_\theta Z \right].$$

Step 2: Gradient Estimation of Integral Terms. For $N_4(\theta)$, noting $\nabla_\theta |\psi|^4 = 2|\psi|^2 \nabla_\theta |\psi|^2 = 4|\psi|^4 O_\theta$

$$(4.14) \quad \nabla_\theta N_4 = \int 4|\psi|^4 O_\theta \, d\mathbf{r} = 4Z \int \frac{|\psi|^2}{Z} (|\psi|^2 O_\theta) \, d\mathbf{r} = 4Z \mathbb{E}[|\psi|^2 O_\theta].$$

Meanwhile, it is known that $\nabla_\theta Z = 2Z \mathbb{E}[O_\theta]$.

Step 3: Substitution and Rearrangement. Substitute the above results back into equation (4.13), and use the relation $\frac{N_4}{Z} = \mathbb{E}[|\psi|^2]$

$$(4.15) \quad \begin{aligned} \nabla_\theta E_{\text{int}} &= \frac{\beta}{2Z^2} \left[4Z \mathbb{E}[|\psi|^2 O_\theta] - 2 \frac{N_4}{Z} (2Z \mathbb{E}[O_\theta]) \right] \\ &= \frac{\beta}{Z} [2\mathbb{E}[|\psi|^2 O_\theta] - 2\mathbb{E}[|\psi|^2] \mathbb{E}[O_\theta]]. \end{aligned}$$

The above equation can also be written in covariance form

$$(4.16) \quad \nabla_\theta E_{\text{int}} = \frac{2\beta}{Z(\theta)} \text{Cov}_{p_\theta}(|\psi|^2, O_\theta).$$

This indicates that the gradient of the interaction energy is driven by the correlation between the wave function density $|\psi|^2$ and the parameter update direction O_θ .

4.2.3. Total Gradient and Local Chemical Potential Synthesis. Combining the linear part (4.11) and the nonlinear part (4.16), the total gradient is

$$(4.17) \quad \begin{aligned} \nabla_\theta E &= 2 \mathbb{E}[(E_L - E_{\text{lin}}) O_\theta] + 2 \mathbb{E} \left[\left(\frac{\beta}{Z} |\psi|^2 - \frac{\beta}{Z} \mathbb{E}[|\psi|^2] \right) O_\theta \right] \\ &= 2 \mathbb{E} \left[\left(\underbrace{E_L + \frac{\beta}{Z} |\psi|^2}_{\mu_L(\mathbf{r})} - \underbrace{\left(E_{\text{lin}} + \frac{\beta}{Z} \mathbb{E}[|\psi|^2] \right)}_{\bar{\mu}} \right) O_\theta \right]. \end{aligned}$$

From this, we naturally derive the definitions of the **Local Chemical Potential** $\mu_L(\mathbf{r})$ and the **Baseline (Mean Chemical Potential)** $\bar{\mu}$

- $\mu_L(\mathbf{r}) = E_L(\mathbf{r}) + \frac{\beta}{Z(\theta)} |\psi_\theta(\mathbf{r})|^2$
- $\bar{\mu} = \mathbb{E}[\mu_L] = E_{\text{lin}} + 2E_{\text{int}}$ (Note the coefficient 2 before E_{int} here)

Finally, we obtain a concise and unified form for the gradient estimator

$$(4.18) \quad \nabla_\theta E(\theta) = 2 \mathbb{E}_{\mathbf{r} \sim p_\theta} [(\mu_L(\mathbf{r}) - \bar{\mu}) \nabla_\theta \ln |\psi_\theta(\mathbf{r})|].$$

4.3. Hybrid Sampling and Algorithm Workflow. Given the explicit dependence on $Z(\theta)$ in equation (4.4), we adopt a “Hybrid Sampling Strategy”

1. **Integration Stream:** Used to calculate the scalar $Z(\theta)$. Since estimating its own normalization constant via samples from p_θ is biased, a base distribution must be used.
2. **MCMC Stream (Gradient Stream):** Used to calculate expectations $\mathbb{E}[\cdot]$. The M-H algorithm is used to generate samples, focusing on regions where the wave function modulus is large to ensure low variance in gradient estimation.

Algorithm 4.1 Neural VMC Optimization Step for GPE

- 1: **Input:** Current parameters θ , MCMC sampler state $\mathcal{X}_{\text{mcmc}}$
- 2: **Step 1: Computation of Normalization Constant Z (Integration Stream)**
- 3: Generate uniform distribution samples $\mathcal{X}_{\text{unif}}$ or construct fixed grid points
- 4: Calculate $Z(\theta) \leftarrow \frac{\text{Vol}(\mathcal{D})}{N_{\text{unif}}} \sum_{\mathbf{r} \in \mathcal{X}_{\text{unif}}} |\psi_\theta(\mathbf{r})|^2$
- 5: **Step 2: Expectation Sampling and Local Quantities (MCMC Stream)**
- 6: Update MCMC state $\mathcal{X}_{\text{mcmc}} \sim |\psi_\theta|^2$ (run k steps of M-H)
- 7: For each sample $\mathbf{r}_i \in \mathcal{X}_{\text{mcmc}}$:
- 8: Calculate local energy $E_L(\mathbf{r}_i)$
- 9: Calculate density contribution $\rho(\mathbf{r}_i) = \frac{\beta}{Z(\theta)} |\psi_\theta(\mathbf{r}_i)|^2$ (using Z from Step 1)
- 10: Calculate local chemical potential $\mu_L(\mathbf{r}_i) = E_L(\mathbf{r}_i) + \rho(\mathbf{r}_i)$
- 11: Calculate log-derivative (Score) $O(\mathbf{r}_i) = \nabla_\theta \ln |\psi_\theta(\mathbf{r}_i)|$
- 12: **Step 3: Gradient Assembly**
- 13: Calculate baseline $\bar{\mu} = \frac{1}{N_s} \sum \mu_L(\mathbf{r}_i)$
- 14: Estimate gradient $\mathbf{g} = \frac{2}{N_s} \sum_{i=1}^{N_s} (\mu_L(\mathbf{r}_i) - \bar{\mu}) O(\mathbf{r}_i)$
- 15: **Step 4: Parameter Update**
- 16: Apply NGD or Adam.

4.4. Computation of the Sobolev Gram Matrix. To implement NGD, the Gram matrix $G(\theta)$ under the X -metric needs to be calculated. This paper chooses the a_ψ -inner product (3.4) at $\hat{\psi}$

$$(4.19) \quad a_{\hat{\psi}}(u, v) = \int_{\mathcal{D}} \left(\frac{1}{2} \nabla u \cdot \nabla v + V(\mathbf{r}) uv + \frac{\beta}{Z(\theta)} |\psi_\theta|^2 uv \right) d\mathbf{r}.$$

The elements of the Gram matrix are defined as the inner products between the tangent vectors of the normalized wave function

$$(4.20) \quad G_{ij}(\theta) = a_{\hat{\psi}} \left(\frac{\partial \hat{\psi}_\theta}{\partial \theta_i}, \frac{\partial \hat{\psi}_\theta}{\partial \theta_j} \right).$$

4.4.1. Centered Representation of Tangent Vectors. First, write the derivative of the normalized wave function $\hat{\psi}_\theta = \psi_\theta / \sqrt{Z}$ with respect to parameter θ_k . Using the log-derivative $O_k(\mathbf{r}) = \partial_{\theta_k} \ln |\psi_\theta(\mathbf{r})|$, we have

$$(4.21) \quad \begin{aligned} \frac{\partial \hat{\psi}_\theta}{\partial \theta_k} &= \frac{\partial}{\partial \theta_k} \left(\frac{\psi_\theta}{\sqrt{Z}} \right) = \frac{(\partial_{\theta_k} \psi_\theta) \sqrt{Z} - \psi_\theta (\frac{1}{2\sqrt{Z}} \partial_{\theta_k} Z)}{Z} \\ &= \hat{\psi}_\theta \left(\frac{\partial_{\theta_k} \psi_\theta}{\psi_\theta} - \frac{1}{2} \frac{\partial_{\theta_k} Z}{Z} \right). \end{aligned}$$

Recalling $\partial_{\theta_k} Z = 2Z\mathbb{E}[O_k]$ and $\partial_{\theta_k} \psi_\theta / \psi_\theta = O_k$, we get

$$(4.22) \quad \frac{\partial \hat{\psi}_\theta}{\partial \theta_k} = \hat{\psi}_\theta(\mathbf{r}) (O_k(\mathbf{r}) - \mathbb{E}_{\mathbf{r} \sim p_\theta}[O_k]) := \hat{\psi}_\theta(\mathbf{r}) \delta O_k(\mathbf{r}).$$

Here $\delta O_k(\mathbf{r})$ is the **Centered Score Vector**, satisfying $\mathbb{E}[\delta O_k] = 0$.

4.4.2. Gradient Expansion of the Kinetic Term. Calculate $\frac{1}{2} \nabla(\partial_{\theta_i} \hat{\psi}) \cdot \nabla(\partial_{\theta_j} \hat{\psi})$. Using expression (4.22) and the product rule

$$(4.23) \quad \nabla \left(\hat{\psi}_\theta \delta O_k \right) = (\nabla \hat{\psi}_\theta) \delta O_k + \hat{\psi}_\theta (\nabla \delta O_k).$$

Defining the **Quantum Force** $\mathbf{F}(\mathbf{r}) = \nabla \ln |\hat{\psi}_\theta(\mathbf{r})| = \frac{\nabla \hat{\psi}_\theta}{\hat{\psi}_\theta}$, and noting $\nabla(\delta O_k) = \nabla(O_k - \text{const}) = \nabla O_k$, the above equation can be rewritten as

$$(4.24) \quad \nabla \left(\frac{\partial \hat{\psi}_\theta}{\partial \theta_k} \right) = \hat{\psi}_\theta(\mathbf{r}) (\mathbf{F}(\mathbf{r}) \delta O_k(\mathbf{r}) + \nabla O_k(\mathbf{r})).$$

Substitute the i and j component gradients into the kinetic integral term K_{ij}

$$(4.25) \quad \begin{aligned} K_{ij} &= \int_{\mathcal{D}} \frac{1}{2} \left[\hat{\psi}(\mathbf{F} \delta O_i + \nabla O_i) \right] \cdot \left[\hat{\psi}(\mathbf{F} \delta O_j + \nabla O_j) \right] \mathrm{d}\mathbf{r} \\ &= \int_{\mathcal{D}} \frac{1}{2} |\hat{\psi}|^2 \left[(\mathbf{F} \cdot \mathbf{F}) \delta O_i \delta O_j + \mathbf{F} \cdot (\delta O_i \nabla O_j + \delta O_j \nabla O_i) + \nabla O_i \cdot \nabla O_j \right] \mathrm{d}\mathbf{r} \\ &= \mathbb{E}_{\mathbf{r} \sim p_\theta} \left[\frac{1}{2} |\mathbf{F}|^2 \delta O_i \delta O_j + \frac{1}{2} \mathbf{F} \cdot (\delta O_i \nabla O_j + \delta O_j \nabla O_i) + \frac{1}{2} \nabla O_i \cdot \nabla O_j \right]. \end{aligned}$$

Here $p_\theta = |\hat{\psi}|^2$ is used to transform the integral into an expectation.

4.4.3. Potential and Interaction Terms. These two terms do not involve spatial derivatives, so we directly substitute the tangent vector $\hat{\psi} \delta O_k$

$$(4.26) \quad \begin{aligned} V_{ij} + I_{ij} &= \int_{\mathcal{D}} \left(V(\mathbf{r}) + \frac{\beta}{Z} |\psi_\theta|^2 \right) (\hat{\psi} \delta O_i)(\hat{\psi} \delta O_j) \mathrm{d}\mathbf{r} \\ &= \int_{\mathcal{D}} |\hat{\psi}|^2 \left(V(\mathbf{r}) + \frac{\beta}{Z} |\psi_\theta|^2 \right) \delta O_i \delta O_j \mathrm{d}\mathbf{r} \\ &= \mathbb{E}_{\mathbf{r} \sim p_\theta} \left[\left(V(\mathbf{r}) + \frac{\beta}{Z(\theta)} |\psi_\theta(\mathbf{r})|^2 \right) \delta O_i(\mathbf{r}) \delta O_j(\mathbf{r}) \right]. \end{aligned}$$

4.4.4. Synthesis and Reorganization. Combine the kinetic, potential, and interaction terms. For brevity, we extract all terms serving as coefficients of $\delta O_i \delta O_j$ and define them as the **Generalized Energy Density Weight** $\mathcal{W}(\mathbf{r})$

$$(4.27) \quad \mathcal{W}(\mathbf{r}) = \underbrace{V(\mathbf{r}) + \frac{\beta}{Z(\theta)} |\psi_\theta(\mathbf{r})|^2}_{\text{Potential and Interaction}} + \underbrace{\frac{1}{2} |\mathbf{F}(\mathbf{r})|^2}_{\text{Drift Kinetic Contribution}}.$$

Finally, the computation formula for the Sobolev Gram matrix G_{ij} is organized

as follows

$$\begin{aligned}
 G_{ij}(\theta) = \mathbb{E}_{\mathbf{r} \sim p_\theta} \left[\underbrace{\mathcal{W}(\mathbf{r}) \delta O_i(\mathbf{r}) \delta O_j(\mathbf{r})}_{\text{Term I: Energy Weighted Fisher Info}} \right. \\
 + \underbrace{\frac{1}{2} \mathbf{F}(\mathbf{r}) \cdot (\nabla O_i(\mathbf{r}) \delta O_j(\mathbf{r}) + \nabla O_j(\mathbf{r}) \delta O_i(\mathbf{r}))}_{\text{Term II: Drift-Gradient Coupling}} \\
 \left. + \underbrace{\frac{1}{2} \nabla O_i(\mathbf{r}) \cdot \nabla O_j(\mathbf{r})}_{\text{Term III: Pure Sobolev Regularization}} \right].
 \end{aligned} \tag{4.28}$$

4.5. Numerical Implementation Details and Techniques. Figure 1 illustrates the overall workflow of the NGD algorithm for solving the GPE based on VMC. To ensure the efficiency and stability of the algorithm on large-scale neural networks, the following techniques are also adopted in the implementation:

1. **Hybrid Mode Automatic Differentiation:** Computing the Gram matrix requires calculating mixed partial derivatives $\nabla_{\mathbf{r}} \nabla_{\theta} \ln |\psi|$. In frameworks like JAX or PyTorch, calculating the full computational graph directly is extremely memory-intensive. We adopt the hybrid mode automatic differentiation strategy proposed by [21]: using Forward-mode AD to calculate low-dimensional spatial derivatives $\nabla_{\mathbf{r}}$, combined with Reverse-mode AD to calculate high-dimensional parameter derivatives ∇_{θ} . Compared to pure reverse mode, this strategy significantly reduces memory consumption and increases computation speed.
2. **Adaptive Damping Strategy:** Due to the over-parameterization of neural networks, the Gram matrix G is often singular or ill-conditioned. We introduce a damping term $(G + \lambda I)^{-1}$ during inversion. The damping coefficient λ has a clear physical meaning: it controls the “Trust Region” of the parameter update under the H^1 norm. We adopt a strategy similar to Levenberg-Marquardt [30], dynamically adjusting λ according to the magnitude of energy decrease.
3. **Physics-Informed Ansatz:** Although Sobolev gradient flow theoretically preserves boundary conditions, hard constraints are more robust in numerical implementation. We construct an ansatz that satisfies boundary conditions:

$$\psi_{\theta}(\mathbf{r}) = \text{Envelope}(\mathbf{r}) \times \text{NN}(\mathbf{r}).$$

For the GPE problem, $\text{Envelope}(\mathbf{r})$ is usually taken as a smoothed form of the Thomas-Fermi approximation or a Gaussian envelope. This not only accelerates convergence but also forces sampling points to be restricted within the physical region, preventing numerical divergence.

4. **Fourier Feature Embedding:** To improve the neural network’s ability to express high-frequency fluctuations, we introduce Fourier feature mapping at the input layer

$$\mathbf{r} \mapsto [\sin(2\pi \mathbf{B}\mathbf{r}), \cos(2\pi \mathbf{B}\mathbf{r})],$$

where \mathbf{B} is a preset frequency matrix [40]. This technique effectively mitigates the spectral bias of neural networks, improving the accuracy of solving for high-frequency wave function morphologies.

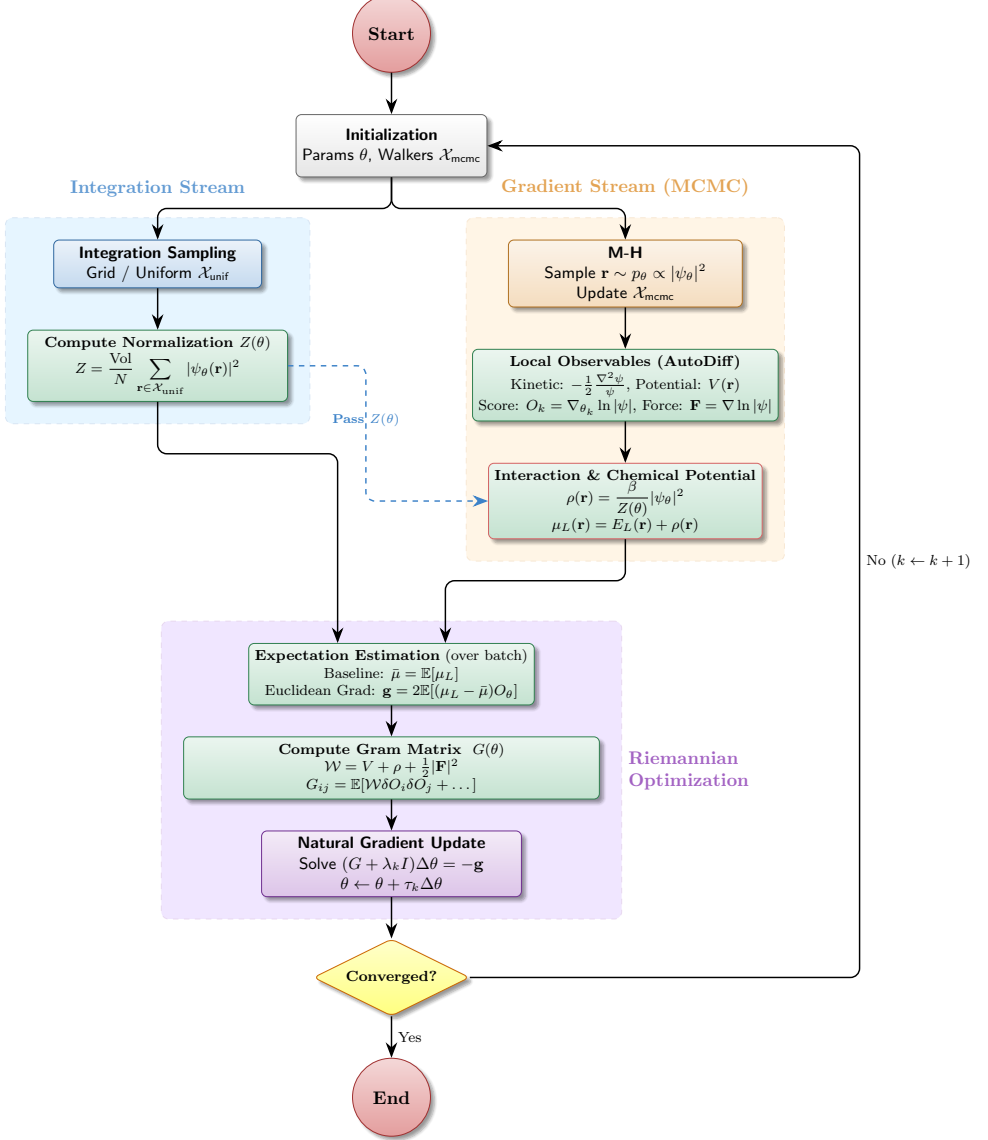


Fig. 1: Workflow of the projected Sobolev NGD methods for the GPE.

5. Numerical Experiments. In this section, we employ the neural VMC method based on NGD to numerically solve classic benchmark problems in the GPE. To comprehensively evaluate the performance advantages of the NGD method in handling strong nonlinear coupling and complex energy landscapes, we compare the experimental results with those of the Adam optimizer.

5.1. Experimental Setup and Evaluation Metrics. To quantitatively measure the degree to which the neural network parameterized wave function $\hat{\psi}_\theta$ satisfies the nonlinear GPE equation, we introduce the **Local Variance of Chemical Potential** as a convergence criterion. For a wave function satisfying the normalization

condition, this metric is mathematically equivalent to the residual norm of the Hamiltonian operator

$$\begin{aligned}
 \text{Res}(\varphi) &= \|H[\varphi]\varphi - \mu_1\varphi\|_2^2 \\
 (5.1) \quad &= \int |\varphi(\mathbf{r})|^2 \left| \frac{H[\varphi]\varphi(\mathbf{r})}{\varphi(\mathbf{r})} - \mu_1 \right|^2 d\mathbf{r} \\
 &= \mathbb{E}_{\mathbf{r} \sim |\varphi|^2} [(\mu_L(\mathbf{r}) - \mu_1)^2] \\
 &= \text{Var}_{\mathbf{r} \sim |\varphi|^2} [\mu_L(\mathbf{r})].
 \end{aligned}$$

The selection of this metric stems directly from the zero variance property in quantum Monte Carlo methods, and its physical connotation includes two aspects

1. **Zero variance of the exact solution:** If $\varphi(\mathbf{r})$ is an exact eigenstate of the GPE, then according to the eigen-equation $H[\varphi]\varphi(\mathbf{r}) = \mu\varphi(\mathbf{r})$, its local chemical potential is defined as $\mu_L(\mathbf{r}) := \frac{H[\varphi]\varphi(\mathbf{r})}{\varphi(\mathbf{r})}$. For the exact solution, $\mu_L(\mathbf{r})$ is constantly equal to the eigenvalue μ over the entire space, so its statistical variance is strictly zero.
2. **Unbiased estimation of approximate solutions:** For a variational approximate solution, the local chemical potential $\mu_L(\mathbf{r})$ fluctuates around the true chemical potential. According to the variational principle, the best unbiased estimator of the minimum eigenvalue (i.e., ground state chemical potential) is given by the expectation value of the operator

$$(5.2) \quad \mu_1 = \langle \varphi | H[\varphi] | \varphi \rangle = \mathbb{E}_{\mathbf{r} \sim |\varphi|^2} [\mu_L(\mathbf{r})].$$

In summary, we take the sample mean of $\mu_L(\mathbf{r})$ as the estimate of μ_1 , while its sample variance $\text{Res}(\varphi)$ measures the deviation of the approximate solution from the eigen-equation.

In addition, to verify the accuracy of the method, we use the high-precision numerical solution calculated by the `DFTK.jl` [24] software package (a direct energy minimization method based on plane wave basis) as the ground truth. We define the following three relative error metrics to evaluate the precision of the neural network from multiple dimensions

$$(5.3) \quad \varepsilon_E = \frac{|E_{\text{NN}} - E_{\text{ref}}|}{|E_{\text{ref}}|}, \quad (\text{Relative Energy Error})$$

$$(5.4) \quad \varepsilon_\mu = \frac{|\mu_{\text{NN}} - \mu_{\text{ref}}|}{|\mu_{\text{ref}}|}, \quad (\text{Relative Chemical Potential Error})$$

$$(5.5) \quad \varepsilon_\rho = \frac{\|\rho_{\text{NN}} - \rho_{\text{ref}}\|_2}{\|\rho_{\text{ref}}\|_2}, \quad (\text{Relative Density } L^2 \text{ Error})$$

where $\rho(\mathbf{r}) = |\varphi(\mathbf{r})|^2$ is the probability density function.

Neural Network Architecture and Hyperparameters. All numerical experiments use a MLP as the wave function ansatz, with the network structure containing 4 hidden layers, each with 64 neurons. The Tanh (hyperbolic tangent) activation function is selected because its smooth and bounded characteristics are well-suited for fitting bound state wave functions with exponential decay. To mitigate the “spectral bias” of neural networks and improve the ability to capture high-frequency spatial details, Fourier feature mapping is introduced at the input layer. Regarding optimization strategies, the learning rate for the Adam optimizer is fixed at 1×10^{-3} ; while the

NGD optimizer uses an adaptive learning rate strategy $\tau_k = \frac{\text{Res}(\varphi)}{1 + \text{Res}(\varphi)}$ to achieve rapid descent in the early training stages and fine searching in the later stages. Similarly, the damping parameter is selected as $\lambda_k = \min(10^{-3}, 10^{-3} \times \text{Res}(\varphi))$.

5.2. Case 1: Harmonic Potential in the Strong Interaction Limit. First, we examine the classic two-dimensional harmonic oscillator potential well $V(\mathbf{r}) = \frac{1}{2}|\mathbf{r}|^2$. As a standard benchmark for numerical simulation of BEC, this case effectively tests the algorithm's performance under different physical mechanisms. The numerical integration domain is set to $\mathcal{D} = [-6, 6]^2$. To fully test the robustness of the algorithm, the dimensionless interaction parameter is set to $\beta \in \{10, 100, 1000\}$, covering the range from weak to strong interactions.

Physical Background and Challenges: As β increases, the strong repulsive interaction between atoms gradually dominates, causing the wave function to broaden outward from the standard Gaussian form of the non-interacting case. Especially in the strong interaction limit of $\beta = 1000$, the system enters the Thomas-Fermi regime, where the kinetic energy term is negligible relative to the potential energy term, and the density distribution exhibits a characteristic inverted paraboloid (flat-top) shape. This transition from a smooth Gaussian distribution to a flat-top distribution with steep edges greatly increases the difficulty of numerical fitting.

Figure 2a shows the evolution of ground state energy with epochs during the NGD optimization process, where the red dashed line represents the reference energy E_{ref} . It can be seen that NGD can rapidly converge the energy to the vicinity of the reference value within very few iteration steps. Figure 2b compares the convergence trajectories of the two optimizers on the local chemical potential variance $\text{Res}(\varphi)$. The results show that the residual descent curve of NGD exhibits a significant steep feature, indicating that it effectively overcomes stiffness in the optimization process by utilizing second-order curvature information, with a convergence rate far exceeding that of the Adam optimizer.

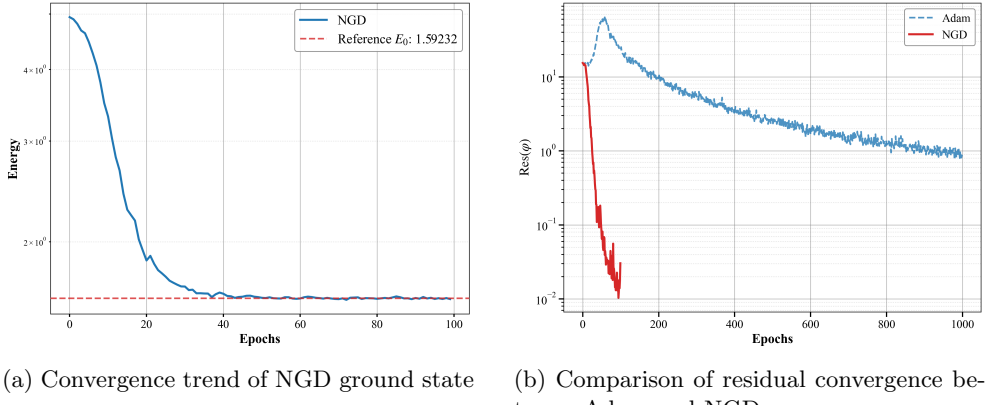


Fig. 2: Convergence analysis of Case 1. (a) Evolution of ground state energy with Epoch during NGD optimization, red dashed line represents reference energy E_{ref} ; (b) Comparison of convergence trajectories of the two optimizers on local chemical potential variance $\text{Res}(\varphi)$.

Figure 3 displays the evolution of ground state density distribution with increasing β and the error distribution between the neural network solution and the reference solution. The error heatmaps in the third column indicate that even when $\beta = 1000$ leads to extremely large gradients at the wave function edges, the NGD method can still accurately capture the flat-top features of the ground state density, keeping the overall error at an extremely low level.

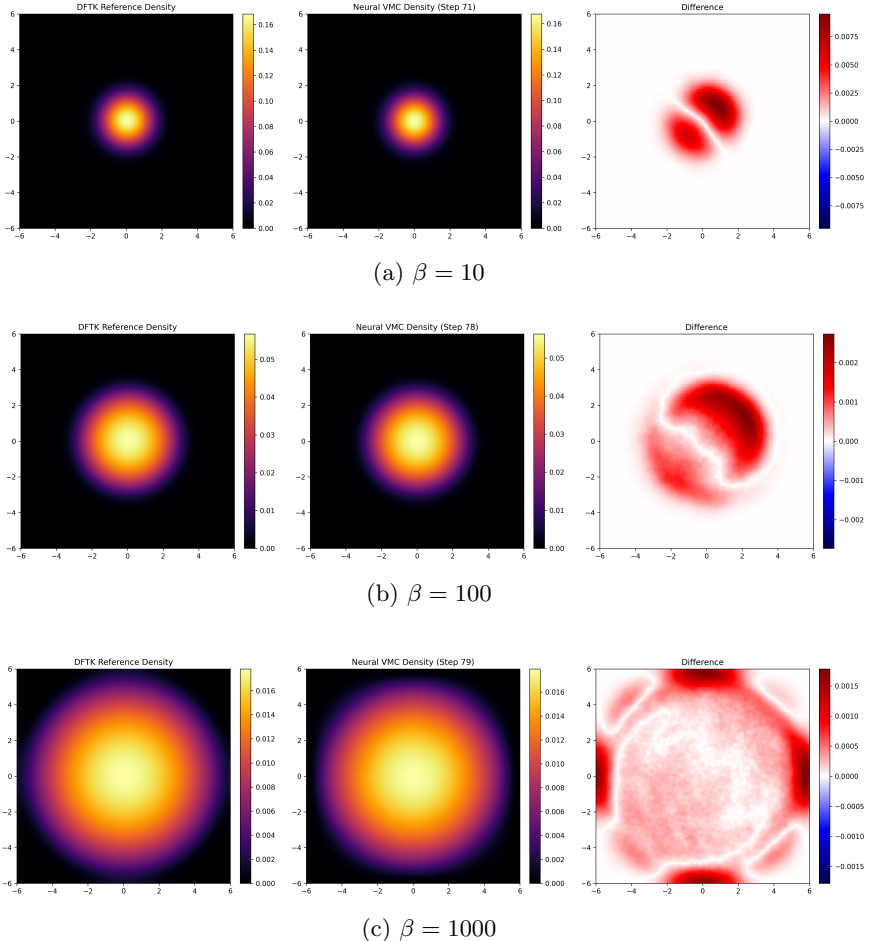


Fig. 3: Evolution of ground state density distribution with interaction strength β in Case 1 (Harmonic potential). First column is reference solution, second column is NGD solution, third column is point-wise error distribution.

Table 1 provides a detailed quantitative comparison of the performance of NGD and Adam optimizers upon reaching the convergence criterion. The experimental results show:

- **Significant improvement in convergence efficiency:** Under all tested β parameters, the number of convergence iterations required by the NGD method is between 70-80 steps, while the Adam optimizer typically requires

600-800 steps. This indicates that after introducing the Riemannian geometric structure using the Fisher information matrix, the convergence speed of NGD is about an order of magnitude faster than traditional first-order methods (Adam).

- **Robustness under strong nonlinearity:** As β increases from 10 to 1000, the system nonlinearity increases significantly, and the optimization landscape becomes ill-conditioned and stiffer. However, the iteration steps of NGD remain highly stable (increasing only from 71 to 79) without significant performance degradation, demonstrating the numerical stability of the natural gradient method when dealing with complex curvature problems.

Table 1: Quantitative comparison of results for Case 1 (Harmonic potential). Here $\varepsilon_E, \varepsilon_\mu, \varepsilon_\rho$ denote relative errors of energy, chemical potential, and density, respectively. Error metrics are presented in scientific notation.

β	Optimizer	Ground State Energy E		Chemical Potential μ		Density ρ		Iter.
		Value	ε_E	Value	ε_μ	ε_ρ		
10	Adam	1.59233	9.8×10^{-6}	2.05165	5.9×10^{-3}	9.3×10^{-2}	810	71
	NGD	1.59231	7.0×10^{-6}	2.06009	1.8×10^{-3}	5.5×10^{-2}		
100	Adam	3.94593	2.4×10^{-6}	5.75283	1.2×10^{-3}	3.2×10^{-2}	688	78
	NGD	3.94553	1.0×10^{-4}	5.73745	3.9×10^{-3}	3.7×10^{-2}		
1000	Adam	11.95900	8.2×10^{-6}	17.93640	5.8×10^{-3}	5.8×10^{-2}	671	79
	NGD	11.96027	1.2×10^{-4}	17.95039	6.6×10^{-3}	4.6×10^{-2}		

5.3. Case 2: Optical Lattice Potential and Multi-scale Structure. Furthermore, we consider the more challenging optical lattice potential problem [22]. This potential consists of a macroscopic magnetic trap potential superimposed with a microscopic periodic lattice, possessing significant multi-scale characteristics

$$(5.6) \quad V(x, y) := V_{\text{ha}}(x, y) + V_{\text{opt}}(x, y),$$

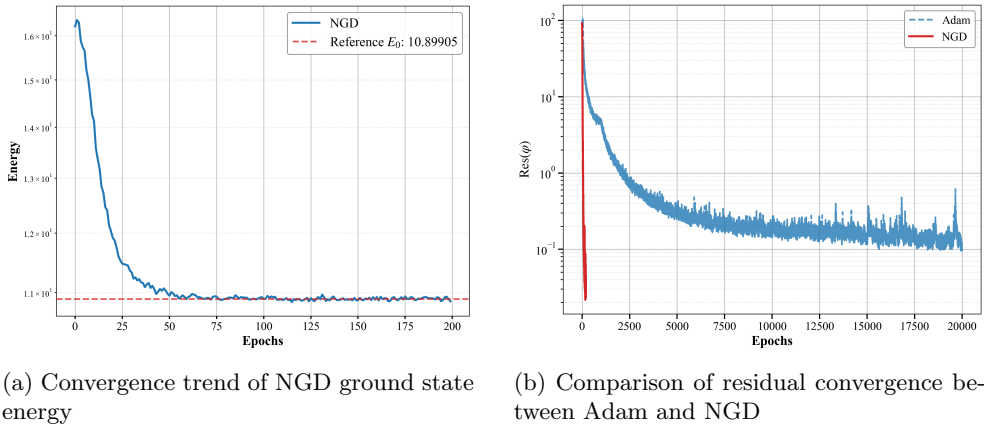
where,

$$(5.7) \quad V_{\text{ha}}(x, y) := \frac{1}{2} (\gamma_x^2 x^2 + \gamma_y^2 y^2), \quad V_{\text{opt}}(x, y) := 10 (\sin^2(\pi x) + \sin^2(\pi y)).$$

In this case, V_{ha} describes an anisotropic harmonic trap with trap frequencies $\gamma_x = 1$ and $\gamma_y = 2$, while V_{opt} simulates an optical lattice field with rapid spatial oscillations. This composite potential field not only contains a large number of local minima (meta-stable states) but also requires the wave function to simultaneously resolve the macroscopic envelope and the density modulation within the microscopic lattice. We set the strong interaction parameter $\beta = 250$ and the computational domain $\mathcal{D} = [-8, 8]^2$.

Figure 4a shows the convergence curve of the ground state energy during NGD optimization, with the red dashed line representing the reference energy E_{ref} . Figure 4b compares the convergence trajectories of the two optimizers. It can be observed that in the face of such a complex multi-scale energy landscape, although the Adam optimizer can descend rapidly in the initial stage, it easily falls into convergence stagnation (Plateau) in the later stage, making it difficult to precisely resolve the subtle

tunneling effects between lattice sites. In contrast, NGD maintains rapid and monotonic convergence characteristics without showing signs of getting trapped in local minima.



(a) Convergence trend of NGD ground state energy

(b) Comparison of residual convergence between Adam and NGD

Fig. 4: Convergence analysis of Case 2. (a) Evolution of ground state energy with Epoch during NGD optimization, red dashed line represents reference energy E_{ref} ; (b) Comparison of convergence trajectories of local chemical potential variance $\text{Res}(\varphi)$ between two optimizers.

Figure 5 visualizes the ground state density distribution obtained by NGD. The results show that NGD successfully captures the localization characteristics of particles at the bottom of the potential wells, and the density distribution exhibits a perfect checkerboard pattern. This indicates that the network not only learned the macroscopic wave packet envelope but also accurately fitted the microscopic periodic modulation caused by the optical lattice, with the wave function maintaining a high degree of overall symmetry.

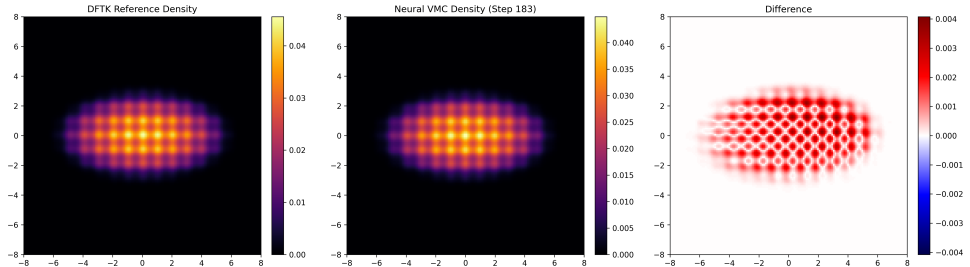


Fig. 5: Visualization results for the optical lattice potential case. The NGD method accurately reconstructs the checkerboard-like periodic modulation of the ground state density.

To quantitatively compare the performance of the two algorithms on multi-scale problems, Table 2 lists detailed error data. It can be seen that in the optical lattice case, the advantage of NGD continues: under the premise of achieving the same or-

der of accuracy (relative error $\sim 10^{-4}$ to 10^{-2}), the iteration efficiency of NGD is significantly higher than that of Adam. This again confirms that introducing second-order optimization information is key to achieving efficient solutions when dealing with physical problems featuring complex geometric structures and multi-scale characteristics.

Table 2: Comparison of calculation results for Case 2 (optical lattice potential, $\beta = 250$).

Optimizer	Ground State Energy E		Chemical Potential μ		Density ρ		Iter.
	Value	ε_E	Value	ε_μ	ε_ρ		
Adam	10.89905	1.0×10^{-7}	13.84491	8.2×10^{-4}	6.4×10^{-2}	18229	
NGD	10.89883	2.0×10^{-5}	13.84366	9.2×10^{-4}	6.2×10^{-2}	183	

Finally, we present the configuration points obtained using MCMC sampling. It can be seen that the sampling points are spatially concentrated in regions where the wave function has significant magnitude, effectively covering the bottom of the potential wells and the tunneling regions between lattice sites, demonstrating stronger adaptive capabilities compared to traditional discretization methods.

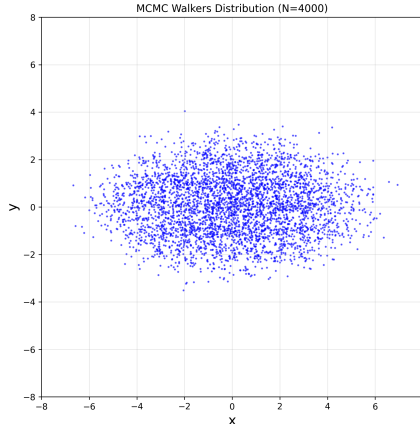


Fig. 6: Spatial distribution of MCMC sampling points in the optical lattice potential case.

6. Conclusion and Outlook. This paper focused on the numerical solution of the ground state of the GPE and proposed a neural VMC algorithm integrating Riemannian geometric optimization theory and deep learning techniques. Following the “optimize-then-discretize” principle, we constructed a theoretically rigorous and numerically efficient geometric optimization framework. The main contributions are summarized as follows: First, at the theoretical level, we utilized the Galerkin projection principle to establish a strict correspondence between the continuous Sobolev

gradient flow on an infinite-dimensional Riemannian manifold and the NGD dynamics in the neural network parameter space. This work provides a solid mathematical foundation for leveraging physically informed second-order metrics within a deep learning framework. Second, at the algorithmic level, addressing the inherent non-convexity and numerical stiffness of the GPE energy functional, we constructed a Sobolev Gram matrix induced by the a_ψ -inner product. This metric implements a physically meaningful preconditioning on the parameter update direction. Furthermore, to solve the problem of explicit dependence on the normalization constant caused by the nonlinear interaction term, we designed a hybrid sampling strategy where the ‘‘Integration Stream’’ and ‘‘MCMC Stream’’ work synergistically, achieving unbiased and efficient estimation of the generalized Fisher information matrix and its gradients. Finally, numerical experiments demonstrate that the proposed projected Sobolev NGD method exhibits excellent performance in challenging benchmark tests such as the Thomas-Fermi regime under the strong interaction limit and multi-scale optical lattice potentials. Compared to standard first-order optimizers like Adam, this method not only reduces the number of iterations required for convergence by an order of magnitude but also exhibits extremely strong robustness in complex energy landscapes, capable of capturing fine spatial structures of wave functions with high precision.

Future research work can focus on the following dimensions:

1. **Rotating BEC and Quantum Vortex Lattice Simulation:** After introducing the rotation term $\Omega \cdot (\mathbf{r} \times \mathbf{p})$, the GPE Hamiltonian breaks real symmetry, and the energy landscape is filled with metastable states corresponding to different vortex configurations. Combining complex-valued neural networks [44] with the Riemannian optimization framework to design algorithms capable of efficiently traversing phase transition points and locking onto dense vortex lattice ground states is a physically significant challenge.
2. **Excited State Solution and Spectral Analysis:** The current framework is mainly limited to ground state solutions. In the future, it can be extended to excited state calculations by combining penalty methods or orthogonal deflation strategies, thereby studying collective excitation modes (such as breathing modes, dipole modes) and energy spectrum characteristics of condensates.
3. **Improvement of Neural Network Architectures:** For large-scale three-dimensional systems or multi-component coupled BECs, MLP with standard initial may face bottlenecks. Exploring network architectures with stronger inductive bias holds promise for further improving sampling efficiency and generalization ability.

REFERENCES

- [1] M. H. ANDERSON, J. R. ENSHER, M. R. MATTHEWS, C. E. WIEMAN, AND E. A. CORNELL, *Observation of bose-einstein condensation in a dilute atomic vapor*, Science, 269 (1995), pp. 198–201.
- [2] X. ANTOINE, A. LEVITT, AND Q. TANG, *Efficient spectral computation of the stationary states of rotating bose-einstein condensates by preconditioned nonlinear conjugate gradient methods*, Journal of Computational Physics, 343 (2017), pp. 92–109.
- [3] V. ARMEGIOIU, J. CARRASQUILLA, S. MISHRA, J. MÜLLER, J. NYS, M. ZEINHOFER, AND H. ZHANG, *Functional neural wavefunction optimization*, arXiv preprint arXiv:2507.10835, (2025).
- [4] W. BAO, Z. CHANG, AND X. ZHAO, *Computing ground states of bose-einstein condensation by normalized deep neural network*, Journal of Computational Physics, 520 (2025), p. 113486.
- [5] W. BAO AND Q. DU, *Computing the ground state solution of bose-einstein condensates by a*

normalized gradient flow, SIAM Journal on Scientific Computing, 25 (2004), pp. 1674–1697.

[6] I. BIOLI, C. MARCATI, AND G. SANGALLI, *Accelerating natural gradient descent for pinns with randomized numerical linear algebra*, arXiv preprint arXiv:2505.11638, (2025).

[7] A. BONFANTI, G. BRUNO, AND C. CIPRIANI, *The challenges of the nonlinear regime for physics-informed neural networks*, Advances in Neural Information Processing Systems, 37 (2024), pp. 41852–41881.

[8] E. CANCÈS, G. KEMLIN, AND A. LEVITT, *Convergence analysis of direct minimization and self-consistent iterations*, SIAM Journal on Matrix Analysis and Applications, 42 (2021), pp. 243–274.

[9] G. CARLEO AND M. TROYER, *Solving the quantum many-body problem with artificial neural networks*, Science, 355 (2017), pp. 602–606, <https://doi.org/10.1126/science.aag2302>.

[10] H. CHEN, G. DONG, W. LIU, AND Z. XIE, *Second-order flows for computing the ground states of rotating bose-einstein condensates*, Journal of Computational Physics, 475 (2023), p. 111872.

[11] Z. CHEN, J. LU, Y. LU, AND X. ZHANG, *On the convergence of sobolev gradient flow for the gross-pitaevskii eigenvalue problem*, SIAM Journal on Numerical Analysis, 62 (2024), pp. 667–691.

[12] G. CYBENKO, *Approximation by superpositions of a sigmoidal function*, Mathematics of control, signals and systems, 2 (1989), pp. 303–314.

[13] I. DANAILA AND P. KAZEMI, *A new sobolev gradient method for direct minimization of the gross-pitaevskii energy with rotation*, SIAM Journal on Scientific Computing, 32 (2010), pp. 2447–2467.

[14] I. DANAILA AND B. PROTAS, *Computation of ground states of the gross-pitaevskii functional via riemannian optimization*, SIAM Journal on Scientific Computing, 39 (2017), pp. B1102–B1129.

[15] F. DANGEL, J. MÜLLER, AND M. ZEINHOFER, *Kronecker-factored approximate curvature for physics-informed neural networks*, Advances in Neural Information Processing Systems, 37 (2024), pp. 34582–34636.

[16] Z. DENIS AND G. CARLEO, *Accurate neural quantum states for interacting lattice bosons*, Quantum, 9 (2025), p. 1772.

[17] C. M. DION AND E. CANCÈS, *Ground state of the time-independent gross-pitaevskii equation*, Computer physics communications, 177 (2007), pp. 787–798.

[18] Z. FENG AND Q. TANG, *On preconditioned riemannian gradient methods for minimizing the gross-pitaevskii energy functional: algorithms, global convergence and optimal local convergence rate*, arXiv preprint arXiv:2510.13516, (2025).

[19] J. J. GARCÍA-RIPOLL AND V. M. PÉREZ-GARCÍA, *Optimizing schrödinger functionals using sobolev gradients: applications to quantum mechanics and nonlinear optics*, SIAM journal on scientific computing, 23 (2001), pp. 1316–1334.

[20] D. J. GRIFFITHS AND D. F. SCHROETER, *Introduction to quantum mechanics*, Cambridge university press, 2018.

[21] A. GUZMÁN-CORDERO, F. DANGEL, G. GOLDSHLAGER, AND M. ZEINHOFER, *Improving energy natural gradient descent through woodbury, momentum, and randomization*, arXiv preprint arXiv:2505.12149, (2025).

[22] P. HENNING AND E. JARLEBRING, *The gross-pitaevskii equation and eigenvector nonlinearities: numerical methods and algorithms*, SIAM Review, 67 (2025), pp. 256–317.

[23] P. HENNING AND D. PETERSEIM, *Sobolev gradient flow for the gross-pitaevskii eigenvalue problem: Global convergence and computational efficiency*, SIAM Journal on Numerical Analysis, 58 (2020), pp. 1744–1772.

[24] M. F. HERBST, A. LEVITT, AND E. CANCÈS, *DFTK: A Julian approach for simulating electrons in solids*, Proc. JuliaCon Conf., 3 (2021), p. 69, <https://doi.org/10.21105/jcon.00069>.

[25] J. HERMANN, Z. SCHÄTZLE, AND F. NOÉ, *Deep-neural-network solution of the electronic schrödinger equation*, Nature Chemistry, 12 (2020), pp. 891–897, <https://doi.org/10.1038/s41557-020-0544-y>.

[26] E. JARLEBRING, S. KVAAL, AND W. MICHELS, *An inverse iteration method for eigenvalue problems with eigenvector nonlinearities*, SIAM Journal on Scientific Computing, 36 (2014), pp. A1978–A2001.

[27] D. P. KINGMA AND J. BA, *Adam: A method for stochastic optimization*, in International Conference on Learning Representations (ICLR), 2015.

[28] Z. KONG, J. Z. YANG, C. YUAN, AND X. ZHAO, *Toward fast, accurate and robust ai prediction of ground states in rotating bec*, arXiv preprint arXiv:2511.07489, (2025).

[29] E. H. LIEB, R. SEIRINGER, AND J. YNGVASON, *Bosons in a trap: A rigorous derivation of the gross-pitaevskii energy functional*, Physical Review A, 61 (2000), p. 043602.

- [30] D. W. MARQUARDT, *An algorithm for least-squares estimation of nonlinear parameters*, Journal of the society for Industrial and Applied Mathematics, 11 (1963), pp. 431–441.
- [31] J. MARTENS, *New insights and perspectives on the natural gradient method*, Journal of Machine Learning Research, 21 (2020), pp. 1–76.
- [32] N. METROPOLIS, A. W. ROSENBLUTH, M. N. ROSENBLUTH, A. H. TELLER, AND E. TELLER, *Equation of state calculations by fast computing machines*, The journal of chemical physics, 21 (1953), pp. 1087–1092.
- [33] L. NURBEKYAN, W. LEI, AND Y. YANG, *Efficient natural gradient descent methods for large-scale pde-based optimization problems*, SIAM Journal on Scientific Computing, 45 (2023), pp. A1621–A1655.
- [34] D. PETERSEIM, J.-F. PIETSCHMANN, J. PÜSCHEL, AND K. RUESS, *Neural network acceleration of iterative methods for nonlinear schrödinger eigenvalue problems*, arXiv preprint arXiv:2507.16349, (2025).
- [35] D. PETERSEIM, J. PÜSCHEL, AND T. STYKEL, *Energy-adaptive riemannian conjugate gradient method for density functional theory*, arXiv preprint arXiv:2503.16225, (2025).
- [36] D. PFAU, J. S. SPENCER, A. G. MATTHEWS, AND W. M. C. FOULKES, *Ab initio solution of the many-electron Schrödinger equation with deep neural networks*, Physical Review Research, 2 (2020), p. 033429.
- [37] M. RAISSI, P. PERDIKARIS, AND G. E. KARNIADAKIS, *Physics-informed neural networks: A deep learning framework for solving forward and inverse problems involving nonlinear partial differential equations*, Journal of Computational physics, 378 (2019), pp. 686–707.
- [38] N. SCHWENCKE, C. ROUSSELOT, A. SHILOVA, AND C. FURTLEHNER, *Amstramgram: Adaptive multi-cutoff strategy modification for anagram*, arXiv preprint arXiv:2510.15998, (2025).
- [39] S. SORELLA, *Green function monte carlo with stochastic reconfiguration*, Physical review letters, 80 (1998), p. 4558.
- [40] M. TANCIK, P. SRINIVASAN, B. MILDENHALL, S. FRIDOVICH-KEIL, N. RAGHAVAN, U. SINGHAL, R. RAMAMOORTHI, J. BARRON, AND R. NG, *Fourier features let networks learn high frequency functions in low dimensional domains*, Advances in neural information processing systems, 33 (2020), pp. 7537–7547.
- [41] L. L. VITERITTI, R. RENDE, AND F. BECCA, *Transformer variational wave functions for frustrated quantum spin systems*, Physical Review Letters, 130 (2023), p. 236401.
- [42] D. WU, R. ROSSI, F. VICENTINI, N. ASTRAKHANTSEV, F. BECCA, X. CAO, J. CARRASQUILLA, F. FERRARI, A. GEORGES, M. HIBAT-ALLAH, ET AL., *Variational benchmarks for quantum many-body problems*, Science, 386 (2024), pp. 296–301.
- [43] M. ZEINHOFER, R. MASRI, AND K.-A. MARDAL, *A unified framework for the error analysis of physics-informed neural networks*, IMA Journal of Numerical Analysis, (2024), p. drae081.
- [44] L. ZHANG, M. DU, X. BAI, Y. CHEN, AND D. ZHANG, *Complex-valued physics-informed machine learning for efficient solving of quintic nonlinear schrödinger equations*, Physical Review Research, 7 (2025), p. 013164.
- [45] A. ZHOU, *An analysis of finite-dimensional approximations for the ground state solution of bose-einstein condensates*, Nonlinearity, 17 (2003), p. 541.